

MAXI J1348–630: Estimating the black hole mass and binary inclination using a scaling technique

Lev Titarchuk^{1,2,3} and Elena Seifina³

¹ Dipartimento di Fisica, University di Ferrara, Via Saragat 1, I-44122, Ferrara, Italy, e-mail: titarchuk@fe.infn.it;

² Astro Space Center, Lebedev Physical Institute, Russian Academy of Science, Profsovnaya ul., 84/32, Moscow, 117997 Russia

³ Lomonosov Moscow State University/Sternberg Astronomical Institute, Universitetsky Prospekt 13, Moscow, 119992, Russia, e-mail: seif@sai.msu.ru

Received ; accepted

ABSTRACT

The multi-wavelength outburst activity in the recently discovered X-ray binary transient MAXI J1348–630 has sparked a great deal of controversy about the characteristics of this binary and questions around whether the source contains a black hole (BH). Here, we present the results of our analysis of the outburst of MAXI J1348–630 using Swift/XRT data. We find that energy spectra in all spectral states can be modeled using a combination of Comptonization and Gaussian iron-line components. In addition, we show that the X-ray photon index, Γ , is correlated with the mass accretion rate, \dot{M} . We find that Γ increases monotonically with \dot{M} from the low-hard state to the high-soft state, and then becomes saturated at $\Gamma \sim 3$. This index behavior is similar to that exhibited by a number of other BH candidates. This result represents observational evidence of the presence of a BH in MAXI J1348–630. We also show that the value of Γ is correlated with the quasi periodic oscillation frequency, ν_L . Based on this correlation, we applied a scaling method to estimate a BH mass of $14.8 \pm 0.9 M_\odot$, using the well-studied BH binary XTE J1550–564 as a reference source. The recent discovery of a giant dust scattering ring around MAXI J1348–630 by SRG/eROSITA has refined distance estimates to this X-ray source. With this distance, we were able to estimate the disk inclination $i = (65 \pm 7)^\circ$ using the scaling technique for the correlation between Γ and normalization proportional to \dot{M} . We detected a specific behavior of the disk seed photon temperature, kT_s , immediately before the outburst: kT_s initially decreases from 0.4 to 0.2 keV and increases only after the source transits to the outburst rise-maximum phase. An initial decrease in kT_s occurred simultaneously with an increase in the illumination fraction, f . We interpreted this effect in terms of the bulk motion Comptonization model. At the start of the outburst, the Compton cloud (or "corona") is very extended and, thus, the seed photons injected to the corona from the relatively far-away disk region, where kT_s is about 0.2–0.4 keV. While \dot{M} increases (or luminosity increases), the corona contracts, thus increasing the seed photon temperature, kT_s . It is possible that such a decrease in kT_s , occurring simultaneously with an increase in the illumination fraction, f , can be considered a signature of the readiness of a BH object to go into an outburst phase.

Key words. accretion, accretion disks – black hole physics – stars, Individual: MAXI J1348–630 – radiation mechanisms

1. Introduction

The X-ray transient MAXI J1348–630 was discovered on January 26, 2019 with the Gas Slit Camera (GSC) of the Monitor of All-sky X-ray Image (MAXI) aboard the International Space Station (Yatabe et al. 2019) and with the Swift/BAT during its X-ray outburst. This outburst lasted for about four months. Further observations made it possible to associate it with an activity of a black hole (BH) located at a distance of 3–4 kpc from the Earth (Tominaga et al. 2020). The X-ray spectral and timing properties of this source estimates have been studied in detail. Combined source spectra in the range of 1–150 keV from Swift/XRT, Swift/BAT, and MAXI/GSC were analyzed by Jana et al. (2020) (hereafter, J20). They appeared in the framework of a two-component advective-flow (TCAF) model whereby the source evolved from the low-hard state (LHS) and through the intermediate state (IS) to the high-soft state [HSS, see, for example McClintock & Remillard (2006); Titarchuk, & Seifina (2009); Shaposhnikov & Titarchuk (2009), hereafter ST09, for definitions of spectral states]. Spectral state evolution of MAXI J1348–630 during its outburst is also confirmed by *NICER* observations [Zhang et al. (2020), hereafter Z20], which is similar to that previously observed for other BH transients.

Two reflares of MAXI J1348–630 were detected, occurring at the end of the main outburst and exhibiting peak fluxes that were one and two orders of magnitude lower than those of the main outburst, respectively, (Z20). These authors showed that the source remained in the hard state during reflares, which were reminiscent of so-called “failed outbursts.” Failed outbursts are usually less bright than regular outbursts at the peak and show no sign of transitions between spectral states (Del Santo et al. 2016; Capitanio et al. 2009; Sturmer & Shrader 2005). This phenomenon was also observed in many BH transients [Stiele & Kong (2016); Furst et al. (2015); Sturmer & Shrader (2005) and ST09]. The study of MAXI J1348–630 with *NICER* and *Swift* also revealed different types of low-frequency QPOs at different phases of outburst (Z20 and J20). In fact, Z20 and J20 also demonstrated it during the source power spectral evolution of MAXI J1348–630, which was also similar to other known BH transients. In Z20 and J20, the results strongly supported a hypothesis that MAXI J1348–630 contained a BH and these authors estimated a BH mass as 8–12 M_\odot (see Table 1). This estimate of a BH mass was made assuming the Shakura-Sunyaev accretion disk (Shakura & Sunyaev (1973), hereafter SS73) and taking into account that the disk temperature, T_d , is inversely

proportional to the fourth root of a BH mass. Thus, Z20 estimated $T_d = 0.5 - 0.7$ keV during the outburst maximum (see also Tominaga et al. (2020)), which is slightly lower than that ($T_d = 0.8 - 1.2$ keV) observed in other BHs during the outburst peak (Dunn et al. 2011). The lower disk temperature of MAXI J1348–630 already indicates that it may harbor a BH with a mass higher than $12 M_\odot$ (Z20 and J20).

Recently, a X-ray spectroscopic analysis of MAXI J1348–630 was performed by Zhang et al. (2022) [hereafter, Z22] using Insight-HXMT and *Swift* data. They found that MAXI J1348–630 demonstrated the peculiar behavior during the outburst rise in 2019. In Z22, the source spectra were fitted by the power-law plus the disk-blackbody components to find that in the soft intermediate and soft states, the object follows to the canonical relation of $L \sim T_d^4$ between the disk luminosity, L , and the peak color temperature, T_d , at a constant inner radius, R_{in} . However, at other phases of the outburst, the behavior is more unusual and strongly deviates from the canonical evolution of known outbursts in BH transients. In particular, in the outburst rise phase, R_{in} is smaller than in the soft state and the temperature, T_d , decreased to 0.5 keV. This contradicts to the standard model of an optically thick inner disk that moves inward at the start of an outburst, becoming monotonically brighter and hotter and replacing the optically thin Comptonization region. Z22 associated this to a decrease in the hardening factor of disk emission with the outburst evolution at the rise phase. In Z22, it was estimated that $T_d = 0.5 - 0.75$ keV during the outburst maximum. This low disk temperature also indicates that MAXI J1348–630 may contain a BH with a mass above $12 M_\odot$, which is consistent with the above conclusions on a BH mass by Z20, J20 and Tominaga et al. (2020).

To date, there are other estimates for the BH mass in MAXI J1348–630 based on a large number of model parameters. In particular, J20 (see section 2 and our Table 1) applied five parameters for a BH mass estimates, such as the Keplerian disk accretion rate (\dot{m} in \dot{M}_{Ed} units), sub-Keplerian halo accretion rate (\dot{m}_h in \dot{M}_{Ed} units), shock location (X_s in units of the Schwarzschild radius $r_s = 2GM_{BH}c^2$), and dimensionless shock compression ratio ($R = r_+/r_-$, the ratio of post-shock matter density to the pre-shock matter density), which are essentially combined with one instrument parameter, namely, the normalization constant (N). Tominaga et al. (2020) use the Kerrbb model (see our Table 1), which gives relations among the spinning parameter, a , inclination angle, i , and a BH mass under a given source distance, mass accretion rate, and spectral hardening factor. In Z20, the authors assumed the closer distance of 3 kpc (also supported by the large observed flux at the soft-to-hard state transition) and an intermediate inclination of 60° , for the average R_{in} in the soft state using their model `tbnew*(simpl*diskbb)`. With their parameters, namely, the disk temperature at the inner radius (T_{in}) in keV, DISKBB normalization (N_{diskbb}), photon index, and scattered fraction (FracScatter), these authors obtained $R_{in} = 110 \pm 5$ km, which is consistent with the ISCO radius for a non-spinning BH of 12 solar masses. Using the MAXI monitoring, Tominaga et al. (2020) utilized the measured evolution of the inner radius of the accretion disk during the soft state to estimate a BH mass (e.g., with an improved distance), however, Lamer et al. (2021) revised their inner disk radius measurements to $R = 97 \pm 13$ km, leading an estimate of a BH mass as 11 ± 2 solar masses using the same model as in (Tominaga et al. 2020).

The BH mass estimates using these methods require an accurate knowledge of the distance to the source. However, the distance to MAXI J1348–630 remains highly debated. Depending on the method of measurement, the distance of MAXI J1348–630 is 3–10 kpc [Nowak (1995); Maccarone (2003); Vahdat

Table 1. Previous BH mass estimates in MAXI J1348–630

Method	M_{BH} , M_\odot	i , deg	d kpc
TCAF model ^a	$9.1^{+1.6}_{-1.2}$...	5–10
Kerrbb model ^b	7	0	4
Luminosity ^c	12	60	3
Luminosity ^d	11 ± 2	...	3.4 ± 0.4

References. (a) Jana et al. (2020); (b) Tominaga et al. (2020); (c) Zhang et al. (2020), and (d) Lamer et al. (2021).

Motlagh et al. (2019); Russell et al. (1974); Tominaga et al. (2020) and J20). In Table 1, we compare all published values of a BH mass and the distance to MAXI J1348–630. Recent observations taken during the first X-ray all-sky survey, using the SGR/eROSITA telescopes installed at the Spektr-RG space observatory, have led to a refined distance of $D_{J1348} = 3.4 \pm 0.4$ kpc (Lamer et al. 2021). This places MAXI J1348–630 in a region of a relatively low stellar density located between the spiral arms of Sagittarius and Centauri of the Milky Way. The new distance estimate has made it possible to now estimate a new BH mass as $11 \pm 2 M_\odot$ (see Table 1) based on the assumption that its companion is a K-type star (Lamer et al. 2021).

The existing estimates for the BH mass in this binary (Table 1) have a large scatter and are often based on a great number of model parameters, therefore these need to be refined. Since there is no dynamical estimate of the BH mass, a re-estimation based on models with a smaller number of parameters, as well as using alternative methods, is desirable. In addition, it is important to prove the presence of a BH in this binary system – not only on the basis of the mass value of the central object ($> 3 M_\odot$) but, for example, using other indicators as well, such as the detection of the constancy (or “saturation”) of the photon index, Γ , versus the mass accretion rate, \dot{M} , during X-ray outburst maximum, which is typical for other reliably established BHs [Stiele et al. (2013) and ST09]. In fact, the index-saturation effect when \dot{M} is increased was already demonstrated in the early work by Titarchuk & Zannias (1998), offering a semi-analytical solution for the full kinetic equation; it was then done using the Monte-Carlo simulations for BH sources (see Laurent & Titarchuk (1999, 2011).

At this point, we can estimate a BH mass in MAXI J1348–630 using the scaling technique. This technique was proposed by Shaposhnikov & Titarchuk (2007) (hereafter ST07) and developed by ST09. It was successfully tested in application to a large number of stellar mass BHs (e.g., Seifina et al. (2014); Titarchuk et al. (2010), ST09, see Fig. 1), as well as intermediate-mass BHs (Titarchuk & Seifina 2016, 2017; Seifina et al. 2017), and supermassive BHs (Seifina et al. 2016; Sobolewska & Papadakis 2009; Giacche et al. 2014; Seifina et al. 2018a,b; Titarchuk, & Seifina 2021).

We note that according to ST07 and ST09, there are two scaling methods: based on the correlation between Γ and the quasi-periodic oscillation frequency (QPO) ν_L ; and based on the correlation between Γ and normalization of the spectrum proportional to \dot{M} (see below Eqs. (1)–(2) for the definition of a mass accretion rate \dot{M}). For the first method ($\Gamma - \nu_L$), obtaining an estimate of the mass of the BH the distance to the source is not required (ST07); whereas for the second method ($\Gamma - \dot{M}$), the source distance and the inclination are needed (ST09).

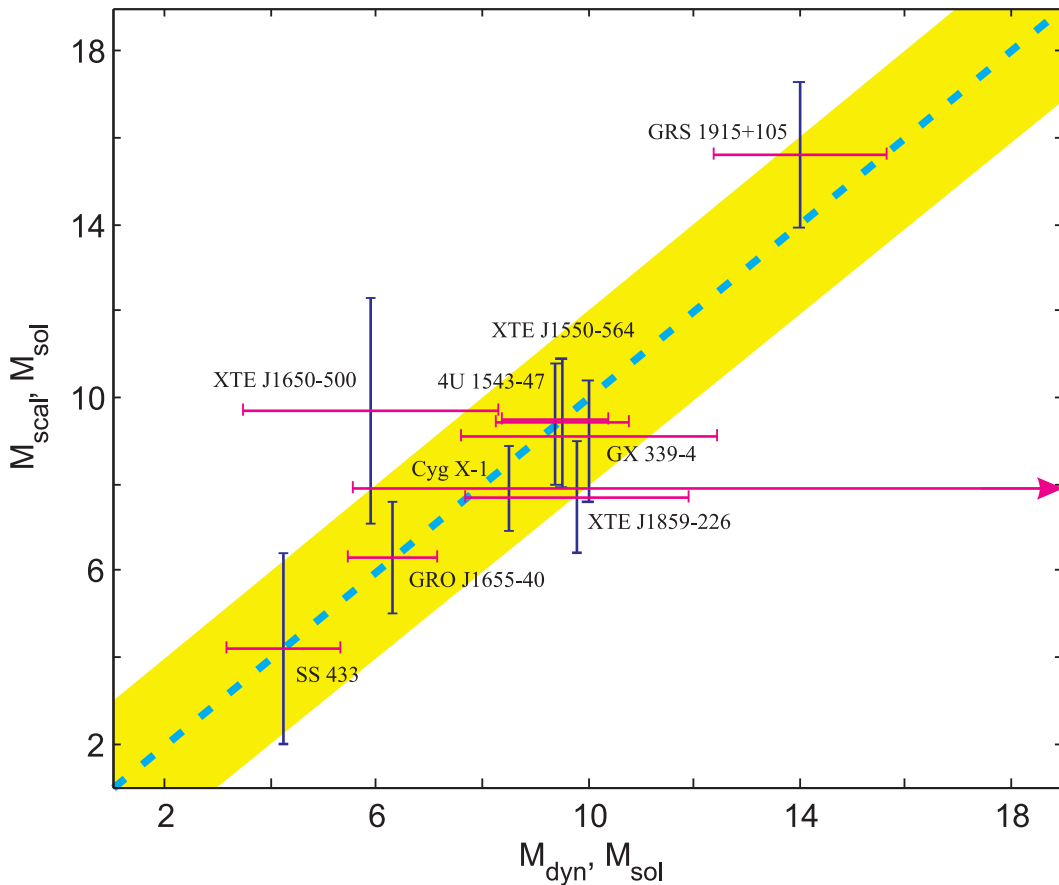


Fig. 1. BH mass from the scaling method (using saturation of the photon index with the mass accretion rate), M_{scal} , compared to the corresponding dynamical masses M_{dyn} for stellar mass BHs. Data are taken from ST09, Shrader & Titarchuk (2003); Shaposhnikov & Titarchuk (2007); Seifina & Titarchuk (2010) (for M_{scal} values), and Greene et al. (2001); Hjellming & Rupen (1995); Herrero et al. (1995); Ninkov et al. (1987); Munoz-Darias et al. (2008); Hynes et al. (2004); Park et al. (2004); Orosz et al. (2002); Sanchez-Fernandez et al. (1999); Sobczak et al. (1999); Petri (2008); Homan et al. (2006); Filippenko & Chornock (2001); Miller-Jones et al. (2021) (for M_{dyn} values). The yellow strip indicates a BH mass spread of $1.3 M_{\odot}$. The deviation from the yellow strip for Cyg X-1 reflects new estimates of the BH mass (marked with a pink arrow), taking into account the strong wind in this binary and possibly associated with the refinement of the source distance (from 2.5 to 2.2 kpc) from the radio data – due to which the BH mass estimate increased in Cyg X-1 from $6.8\text{--}13.3 M_{\odot}$ to $21 M_{\odot}$ (Miller-Jones et al. 2021).

For both methods, it is important for the source to show a change in spectral states during the outburst and a characteristic behavior of Γ ; namely, a monotonic increase of Γ with ν_L or \dot{M} in the LHS→IS→HSS transition and reaching a constant level (saturating) at high values of ν_L or \dot{M} . The saturation of Γ (i.e., the so-called “ Γ -saturation phase”) during the outburst is a specific signature that supports the notion that this particular object containing a BH (Titarchuk & Zannias 1998). Indeed, the Γ -saturation phase can be caused only by an accretion flow converging to the event horizon of a BH (see the Monte-Carlo simulation results in Laurent & Titarchuk (1999, 2011)).

The scaling method has advantages in determining a BH mass, namely: using X-ray data associated with the innermost regions of the accretion disk carry the direct information about a BH and consequently, an estimate of a BH mass is independent of the distance to the object and its inclination [using ($\Gamma - \nu_L$) correlation].

In this paper, based on *Swift* data analysis, we estimate a BH mass in MAXI J1348–630 and the system’s inclination, by applying the scaling technique. In §2 we provide details of our data analysis, while in §3.1 we present a description of the spectral models used to fit these data. In §3.2.1–3.3 we focus on observational results and their interpretation. In §4 we discuss the main results of the paper. In §5 we present our final conclusions.

2. Data Reduction

Using *Swift*/XRT data in the 0.3–10 keV energy range, we analyzed a total of 53 observations of the X-ray transient MAXI J1348–630 during its outburst from January 26 to September 8, 2019. In Table 2, we report the log of observations for MAXI J1348–630 used in our study.

The data were processed using the HEASOFT v6.14, the tool *xrtpipeline* v0.12.84 and the calibration files (CALDB version 4.1). The ancillary response files were created using *xrtmkarf* v0.6.0 and exposure maps generated by *xrtexpomap* v0.2.7. Source events were accumulated within a circular region with radius of 20 pixels (1 pixel = 2.35 arcsec) centered at the position of MAXI J1348–630 [$\alpha=13^h48^m12^s.7$ and $\delta=-63^{\circ}16'26''.8$, see Kennea & Negoro (2019)] when the X-ray source was faint (see low-count plateau in Fig. 3). In the peak phase of the outburst (MJD 58510 – 58606), when the source became extremely bright and a pile-up effect occurred, we used an annulus extraction region with variable inner and outer radius (see column 11 in Table A1) to attenuate this problem (Vaughan et al. 2006). We used XRT data both in the Windowed Timing (WT) mode during the bright part of the outburst (MJD 58509 – 58720) and in the Photon Counting (PC) mode for the remaining observations when the X-ray source became sufficiently

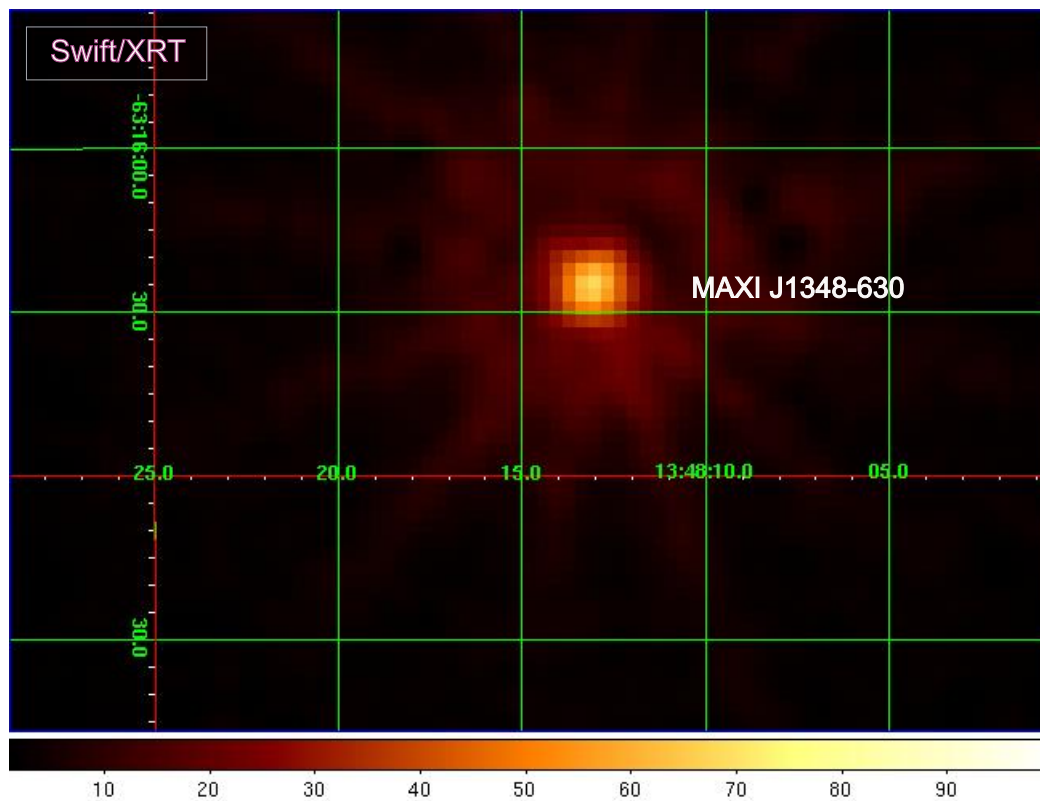


Fig. 2. Swift/XRT (0.3–10 keV) image of MAXI J1348–30 accumulated from January 26, 2019 to October 17, 2020 with an exposure of 52 ks.

faint (≤ 1 count/s). The background was estimated in a nearby source-free circular region. Using `xselect v2.4` task, the source and background light curves (0.01 s time resolution) and spectra were generated. The spectra were re-binned with 20 counts in each energy bin using the `grppha` task in order to apply χ^2 -statistics. We also used the online XRT data product generator¹ to obtain the image of the source field of view in order to make a visual inspection and to get rid of a possible contamination from

¹ http://www.swift.ac.uk/user_objects/

nearby sources (Evans et al. 2007, 2009). In Figure 2, we show an adaptively smoothed *Swift*/XRT (0.3 – 10 keV) image of the MAXI J1348–630 field, obtained from 2019 January 26 to 2020 October 17, with an exposure of 52 ks during MAXI J1348–630, when it was in outburst and quiescent states.

The evolution of Swift/XRT in 0.3–10 keV energy range during 58450–58800 MJD observations is presented in the top panel of Fig. 3. We also obtained 1-day bin MAXI light curves from the 2–20 keV band as well as the 2–4 keV, 4–10 keV and 10–20

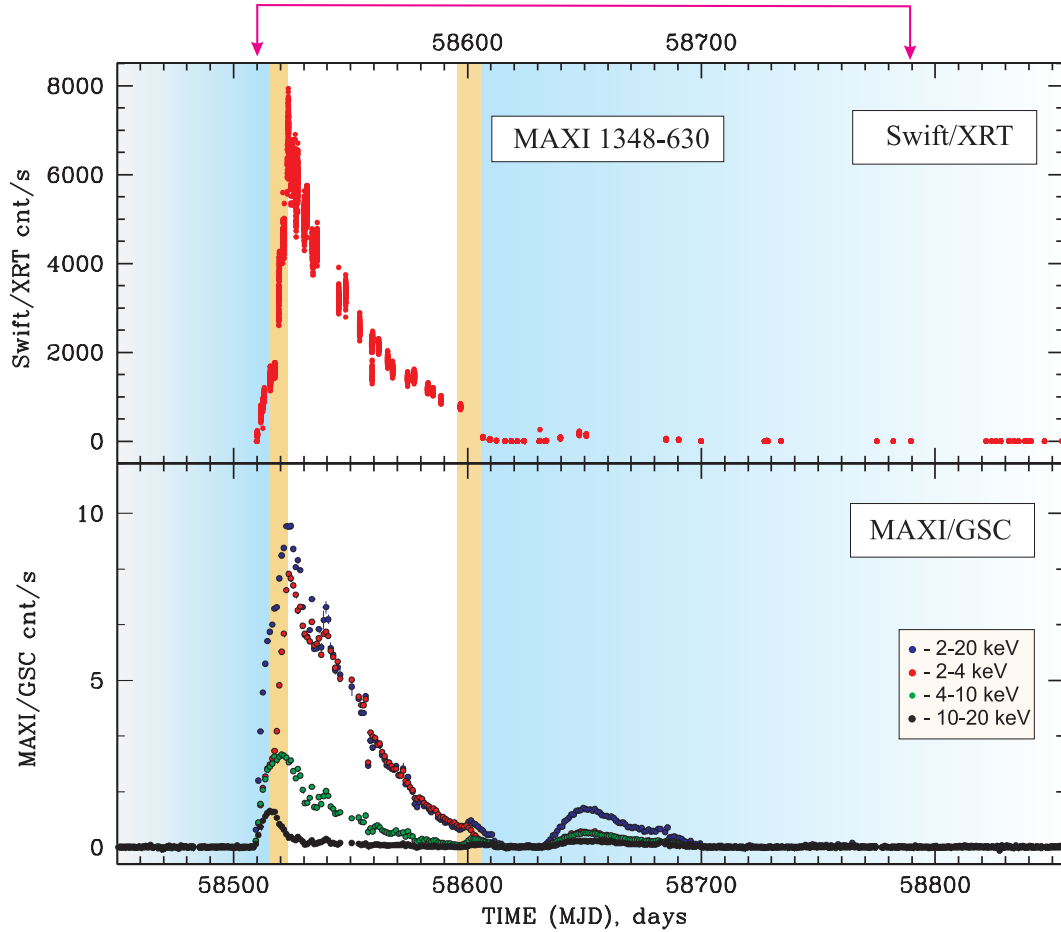


Fig. 3. Evolution of Swift/XRT (0.3–10 keV, *top panel*) and MAXI/GSC flux (*bottom panel*) in 2–20 keV, 2–4 keV, 4–10 keV and 10–20 keV energy ranges during 58450–58800 MJD observations of MAXI J1348–630. Vertical bright blue, hazel, and white strips indicates the LHS, IS and HSS spectral states, correspondingly (for identification of spectral states see Sec. 3.1). Pink arrow (at top of the panel) indicate the time interval under our study (from January to September, 2019) for data sets listed in Table 2.

keV bands (Fig. 3, bottom panel), through the MAXI ondemand Web interface².

Only one outburst of this object is known to date (Fig. 3), when it showed a rapid increase in X-ray luminosity (on the order of 10 days, during outburst rise phase) before reaching its

peak luminosity, then followed by a slow luminosity decline over about four months (outburst decay phase). During this active phase, we can see transitions between different spectral states (see color strip indications in Fig. 3).

² <http://maxi.riken.jp/pubdata/v6m/J1348-632/index.html>

Table 2. List of *Swift* observations of MAXI J1348–30 used in our analysis

Obs. ID	Start time (UT)	End time (UT)	MJD interval
00885807000 ^{1,2,5}	2019 Jan 26/12:07:07	2019 Jan 26 20:11:45	58509.47 – 58509.84
00885960000 ^{1,5}	2019 Jan 27 00:59:29	2019 Jan 27 00:59:35	58510.04 – 58510.05
00886266000 ^{1,5,6}	2019 Jan 28 15:05:37	2019 Jan 28 15:08:13	58511.58 – 58511.63
00886496000 ^{1,5,6}	2019 Jan 29 10:24:54	2019 Jan 29 10:25:01	58512.43 – 58512.44
00011107(001 ^{1,5,6} ,002 ^{3,4,5,6} ,003 ^{3,6} -023 ^{5,6} ,024 ^{4,5,6} , 025-028,029 ^{4,5,6} ,036 ^{1,5} , 037-055 ⁵)	2019 Jan 30	2019 Sep 8	58513.11 – 58734.02
00088843(001-002) ^{1,5}	2019 Feb 1	2019 Mar 8	58515.75 – 58550.47

References. (1) Jana et al. (2020); (2) Kennea & Negoro (2019); (3) Bassi et al. (2019); (4) Tominaga et al. (2020); (5) Carotenuto et al. (2021b) and (6) Zhang et al. (2022).

3. Analysis and results

In this section, we present the results of spectral analysis during the 2019 outburst of MAXI J1348–630 observed by *Swift*/XRT. In particular, we analyze how the X-ray spectrum of the source behaves, especially Γ , during the outburst from MJD 58509 to 58734 MJD.

3.1. Spectral analysis

To fit the energy spectra of this source, we used a XSPEC model consisting of the Comptonization (bulk-motion Comptonization, hereafter BMC) component [see Titarchuk & Zannias (1998); Laurent & Titarchuk (1999)] and the iron line (Gaussian) components. We also used a multiplicative tbabs model (Wilms et al. 2000), which takes into account absorption by neutral material. We assume that accretion onto a BH is described by two main zones [see, for example, Fig. 1 in Titarchuk, & Seifina (2021)]: a geometrically thin accretion disk, such as the standard Shakura-Sunyaev disk, (see SS73), and a transition layer (TL), which is an intermediate link between the accretion disk, and a converging (bulk) region (see Titarchuk & Fiorito (2004)). The latter is assumed to exist, at least below 3 Schwarzschild radii, $3R_S = 6GM_{\text{BH}}/c^2$. The spectral model parameters are the equivalent hydrogen absorption column density, N_H ; the photon index, Γ ; whereas $\log(A)$ is related to the Comptonized factor, $f [= A/(1+A)]$, and the color temperature and normalization of the seed photon blackbody component, kT_s and N_{bmc} , respectively. The Comptonized component is additively combined with the gaussian line model for which the fit parameters are the line energy, E_{line} , and normalization, N_{line} . The centroid of the gaussian (Fe K_α) line can vary from 6.3 to 6.9 keV; the Fe line width was varied from 0.1 to 1 keV and then subsequently fixed at 0.5 keV (as the best-fit value). The parameter $\log(A)$ of the BMC component is fixed at 2 when the best-fit $\log(A) \gg 1$. In fact, for a sufficiently high $\log(A) \gg 1$ (and, therefore, a high value A), the illumination factor $f = A/(1+A)$ becomes a constant value close to 1 (that is, the same as in the case of $\log(A) = 2$). N_H was fixed at the level of $0.64 \times 10^{22} \text{ cm}^{-2}$ (Z20).

Similarly to the ordinary bbody XSPEC model, the BMC normalization is a ratio of the source (disk) luminosity L to the square of the distance, d (ST09, see Eq. 1 in that work):

$$N_{\text{bmc}} = \left(\frac{L}{10^{39} \text{ erg/s}} \right) \left(\frac{10 \text{ kpc}}{d} \right)^2. \quad (1)$$

This encompasses an important property of the BMC model. That is to say that using this model can lead to a correct evaluation of the normalization of the original “seed” component,

which is presumably a correct \dot{M} indicator (Seifina & Titarchuk 2011). In turn, we have:

$$L = \frac{GM_{\text{BH}}\dot{M}}{R_*} = \eta(r_*)\dot{m}L_{\text{Ed}}. \quad (2)$$

Here $R_* = r_*R_S$ is an effective radius where the main energy release takes place in the disk, $R_S = 2GM/c^2$ is the Schwarzschild radius, $\eta = 1/(2r_*)$, $\dot{m} = \dot{M}/\dot{M}_{\text{crit}}$ is the dimensionless \dot{M} in units of the critical mass accretion rate, $\dot{M}_{\text{crit}} = L_{\text{Ed}}/c^2$, and L_{Ed} is the Eddington luminosity. For the formulation of the Comptonization problem, we can look to Titarchuk et al. (1997); Titarchuk & Zannias (1998); Laurent & Titarchuk (1999); Borozdin et al. (1999); Shaposhnikov & Titarchuk (2009).

The best-fit model parameters for all states are shown in Table A. A systematic uncertainty of 1% is intended to represent the instrumental flux calibration uncertainty and has been applied to all analyzed *Swift* spectra. A spectral analysis of the *Swift*/XRT data fits of MAXI J1348–630, in principle, can provide a general picture of the spectral evolution. We can trace the change in the spectrum shape during the LHS-IS-HSS transition in Fig. 4, which demonstrates three representative $E * F_E$ spectral diagrams for different states of MAXI J1348–630. To identify the spectral states, we relied on the best-fit value of the photon index: LHS ($\Gamma < 1.6$), IS ($1.6 < \Gamma < 1.8$) and HSS ($\Gamma > 1.8$). The emergent spectra (see Fig. 4) can be described as a sum of the low-energy blackbody and its fraction convolved with the Comptonization Green function (CGF) [see Eqs. (16) and (B5) in Sunyaev & Titarchuk (1980)]. The HSS and IS spectra are characterized by a strong soft blackbody component (presumably related to the accretion disk) and a power law (as the hard tail of the CGF). In the LHS, the Comptonization component is dominant and the blackbody component is barely seen because the innermost part of the disk is fully covered by the scattering media which has a Thomson optical depth more than 2.

The general picture of the LHS-IS-HSS transition is illustrated in Figure 5, where we put together spectra of the LHS, IS, and HSS, to demonstrate the source spectral evolution from the high-soft to low-hard states based on the *Swift* observations. Here, the data are presented in the left panel for LHS, taken from observations 0008884300 (bright blue), 0088496000 (red) and 0088596000 (pink); at the right panel for IS, we have 00011107003 (black), and 0088826000 (orange) as well as for HSS [00011107007 (blue)]. We should point out the fact that the HSS and IS spectra are characterized by a strong soft blackbody component and a power law extending up to 10 keV, while in the LHS spectrum, the Comptonization component is dominant and the blackbody component is barely seen.

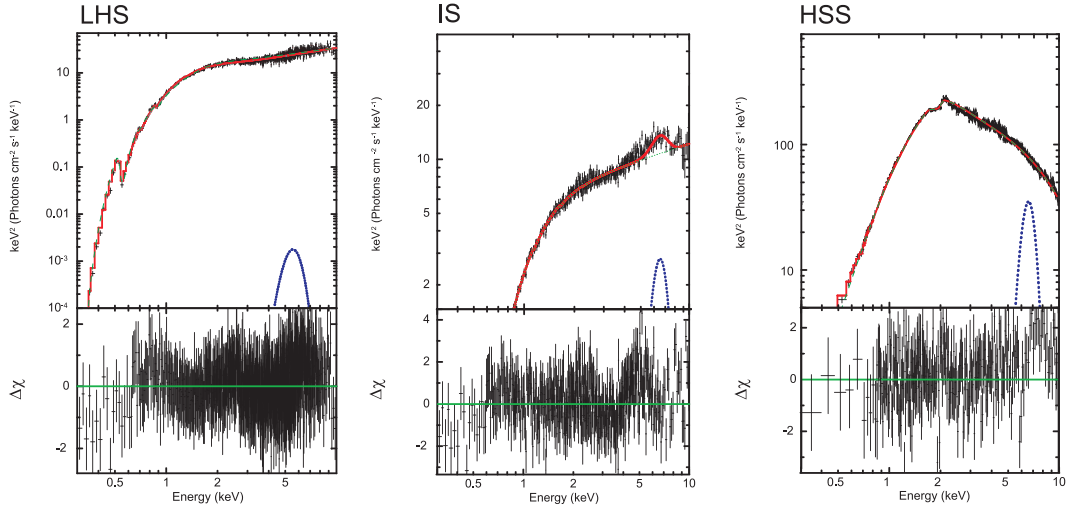


Fig. 4. Evolution of MAXI J1348–630 spectra, fitted using the `tbabs*(bmc+gauss)` model for three spectral states. Data are taken from the *Swift*/XRT observations: 00088843001 (MJD=58515.75, left), 00011107003 (MJD=58519, center), and 00011107007 (MJD=58524, right). Data are shown as black crosses and the spectral model components are displayed as dashed green and blue lines for the BMC and gaussian components, respectively. The resulting spectrum as a sum of these components are presented by red line. In the bottom panels, we show the corresponding $\Delta\chi$ versus photon energy (in keV).

An analysis of the *Swift*/XRT data fits (see Figure 6 and Table A) showed that Γ monotonically increases from 1.1 to 3 (red points in Fig. 6), when the normalization of the BMC component (or \dot{M}) increases by a factor of 10 (green points, in Fig. 6) at the outburst rise phase (LHS-IS, MJD 58509–58512). At the rise-phase start of the outburst (LHS, MJD 58509 – 58519), the

spectra are gradually softened with a increase in the total flux and Γ slowly increases from 1.1 to 2, together with a slight decrease in the disk seed photon temperature, kT_s , from 0.45 to 0.2 keV (black points, in Fig. 6). In this case, the contribution of the Comptonized component, f , to the total flux increased from 0.7 to 0.9 (blue points, in Fig. 6). Furthermore, at the end of

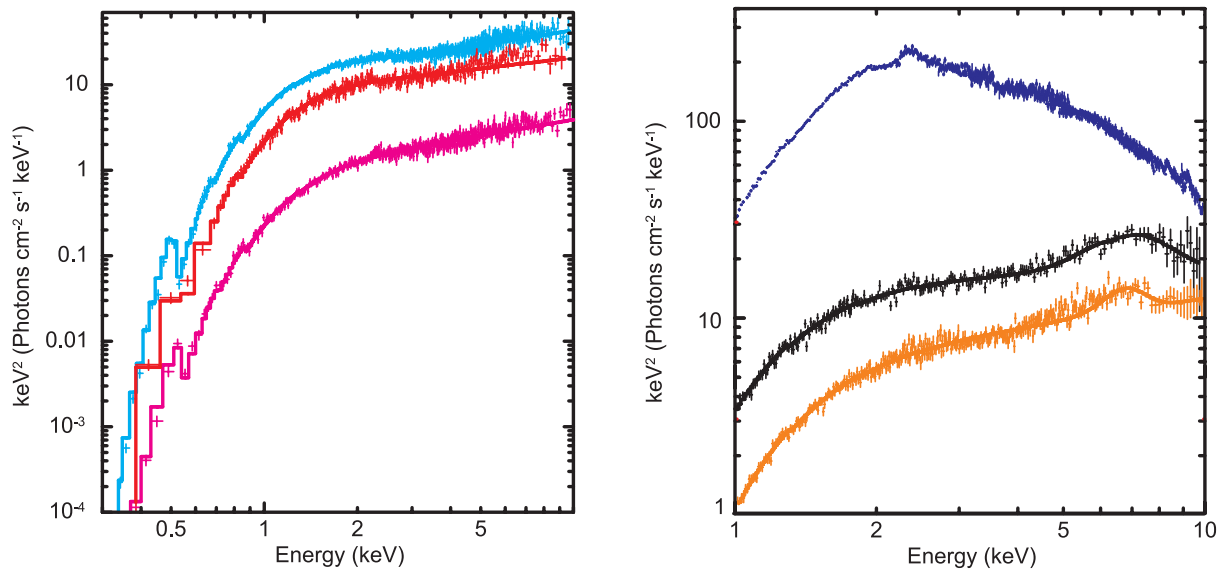


Fig. 5. Six representative EF_E spectral diagrams during different spectral states of MAXI J1348–30. Left panel: Data taken from *Swift/XRT* observations 0008884300 (bright blue, LHS), 0088496000 (red, LHS), and 0088596000 (pink, LHS). Right panel: Data taken for 00011107003 (black, IS), 0088826000 (orange, IS), and 00011107007 (blue, HSS).

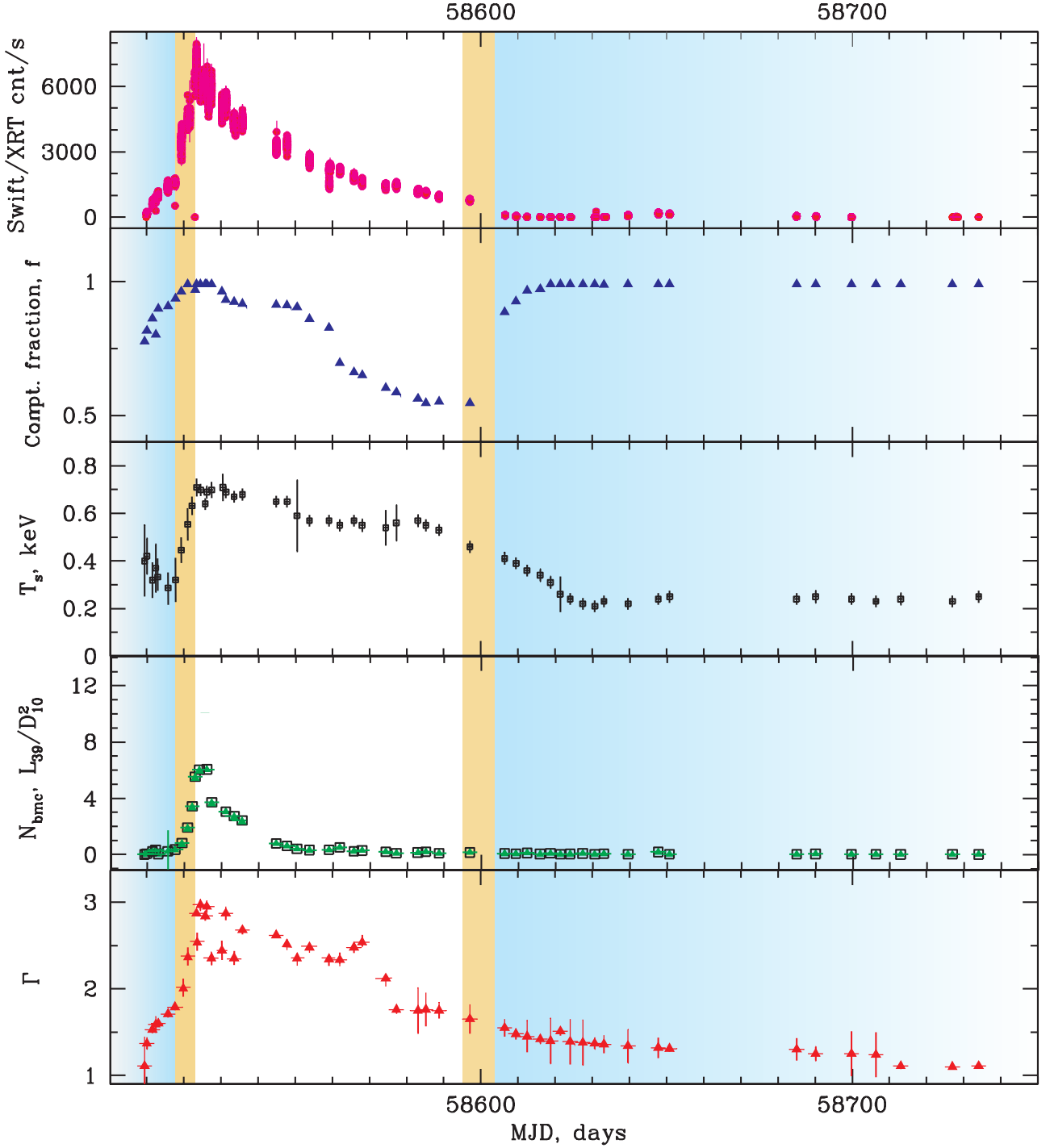


Fig. 6. Temporal evolution of the Swift/XTE count rate (pink) from the LHS to the HSS and back, shown from top to bottom. Comptonized fraction f (blue), seed photon temperature T_s (black), N_{bmc} (green) and Γ (red) during the MJD=58509–58734 outburst transition set. We note that the Comptonized fraction $f = A/(A + 1)$ characterizes the fraction of the soft photons illuminating the Compton cloud (CC), and subsequently up-scattered in the CC hot plasma. Vertical bright blue, hazel and white strips indicates the LHS, IS, and HSS spectral states, correspondingly (as in Fig. 3).

the outburst-rise phase (HSS, MJD 58519 – 58525), the spectra further softened, with an increase in the total flux, and Γ continued to increase from 2 to 3, along with a slight increase in the disk seed photon temperature, kT_s , from 0.2 to 0.75 keV. At the same time, the contribution of the Comptonized component, f , to the total flux remained almost constant, increasing from 0.9 to 1 (blue dots, in Fig. 6). This interesting behavior of kT_s and f at the beginning of the outburst is further discussed in Sect. 4.

In turn, at the decay phase of the outburst (HSS, MJD 58525–58597), the spectra are gradually hardened, with a decrease in the total flux, and Γ slowly decreases from 3. to 1.7, together with a slight decrease in the disk seed photon temperature kT_s from 0.7 to 0.5 keV (black points, in Fig. 6). In this case, the contribution of the Comptonized component, f , to the total flux decreased from 1 to 0.5 (blue points, in Fig. 6). When the source passed from the IS to the LHS (MJD 58612), the temperature,

kT_s , dropped to ~ 0.25 keV, and Γ decreased to $\Gamma \sim 1.4$, while the contribution of the Comptonized component to the total flux increased to $f = 1$. After the source returned to the LHS (MJD 58606), the Comptonized component ($f = 1$) prevailed in the spectra, while Γ changed in the interval 1.1–1.4 and kT_s was about 0.2 keV.

3.2. BH mass estimate

The previous BH mass estimates were made based on luminosity determination or were based on the TSAF/Kerrbb spectral model fitting [see Tominaga et al. (2020); Russell et al. (1974); Nowak (1995); Maccarone (2003); Vahdat Motlagh et al. (2019); Lamer et al. (2021) and J20]. It is worth noting that a BH mass estimate using these methods turns out to be highly dependent on the accuracy of the distance to the source.

Now, we go on to estimate the BH mass (M_{J1348}) using scaling methods developed by ST09, based on $\Gamma - \nu_L$ (see our Sect. 3.2.1) and $\Gamma - N_{bmc}$ (Sect. 3.2.2) correlations for the target source and the reference source. By using the $\Gamma - \nu_L$ correlation, we deal with the method that offers the advantage of being independent of the binary inclination and source distance.

3.2.1. Scaling of Γ vs ν_L correlation for MAXI J1348–630

We obtained an estimate of a BH mass in MAXI J1348–630 using the results of timing analysis by Z20 (see their Table 1) in comparison with our results of spectral analysis for the close MJD dates (Table A.1). We obtained the Γ dependence on ν_L and demonstrated that Γ for MAXI J1348–630 is correlated with ν_L and saturated at $\Gamma = 2.9 \pm 0.1$ at frequencies above 6 Hz (see Fig. 7)³

In order to estimate M_{J1348} , we chose Galactic source XTE J1550–564 as the reference source (see a detailed explanation of the scaling method in ST09). It is worth noting that XTE J1550–564 is a source with the well-known parameters of the reference source: the spatial orientation (the inclination i_r), BH mass (m_r), and distance (d_r) were determined by a dynamic method (see Table 3 and Orosz et al. (2002)). Figure 7 shows that $\Gamma - \nu_L$ correlations for MAXI J1348–630 and XTE J1550–564 follow a similar pattern of Γ with ν_L : it is linear and monotonically increases until it reaches a transition frequency, ν_{tr} ; whereas around ν_{tr} the function $\Gamma - \nu_L$ smoothly transitions into a horizontal line. It becomes a constant at a value 2.9 ± 0.1 , which we assume to be the Γ saturation.

This behavior is well reproduced by the analytical function $f(\nu)$ (see ST09):

$$f(\nu) = A - (D \cdot B) \ln \left(\exp \frac{\nu_{tr} - \nu}{D} + 1 \right). \quad (3)$$

Using this function, $f(\nu)$, we fit the observed $\Gamma - \nu_L$ correlations applying the least-squares method. Specifically, we minimized the sum of squared residuals of the function $f(\nu, A, B, D, \nu_{tr})$ from the observed $\Gamma - \nu_L$ track by selecting values of the parameters A, B, D, ν_{tr} for which this function, $f(\nu, A, B, D, \nu_{tr})$ is closest to the observable $\Gamma - \nu_L$ correlation.

The significance of the parameters A and B follows from the asymptotic of the function $f(\nu)$. For $\nu \ll \nu_{tr}$ we see that B is the slope of the correlation. On the other hand, for $\nu \gg \nu_{tr}$ the function $f(\nu)$ equals to A . From this it is immediately clear that

³ Hereafter, we consider the term of the Γ saturation as a constant of Γ in the $\Gamma - \nu_L$ correlation track at high values of ν_L .

the parameter A is a value of the Γ -saturation level. We introduced the parameter D in order to control how fast the transition occurs.

Results after fitting the $\Gamma - \nu_L$ correlations for these sources using Eq. (3), presented in Table 4, where $A = 2.94 \pm 0.08$, $B = 1.27 \pm 0.01$, $\nu_{tr} = 10.1 \pm 0.5$ Hz and $A = 2.93 \pm 0.09$, $B = 1.25 \pm 0.04$, $\nu_{tr} = 6.48 \pm 0.07$ Hz for XTE 1550-564 and MAXI J1348–630, respectively. It is worth noting all these parameters are relatively close to each other. Numerous fit tests have shown that parameter D varies slightly around 1 Hz, so we fixed it at 1.0 Hz for the convenience of the fitting procedure. We fit the correlations in order to get these parameters, A, B, D , and ν_{tr} (see Table 4), and thus to obtain the scaling factor, s_ν [Eqs. (4) and (5)]. Finally, we estimated the BH mass in MAXI J1348–630 applying the scaling method (see ST09, Eq. 2 therein):

$$M_t = s_\nu \times M_r, \quad (4)$$

where

$$s_\nu = \nu_{tr,r} / \nu_{tr,t} \quad (5)$$

is the scaling factor and subscripts r and t denote the reference and target sources.

For the reference source, we chose the data from the rise of the 1998 XTE J1550–564 outburst, because its Γ -saturation level is approximately that of MAXI J1348–630, $\Gamma_{sat} = 2.9 \pm 0.1$. The best-fit curves are shown by blue and red lines in Fig. 7. The inferred uncertainty (error bar) of M_{J1348} is mostly affected by scattering and error bars of the $\Gamma - \nu_L$ points.

As a result, the BH mass in MAXI J1348–630 is

$$\begin{aligned} M_{J1348} &= s_{J1550 \rightarrow J1348} * M_{J1550} = \\ &= \frac{(\nu_{tr,J1550}/10.1Hz)}{(\nu_{tr,J1348}/6.5Hz)} (M_{J1550}/9.5M_\odot) = 14.8 \pm 0.9M_\odot, \end{aligned} \quad (6)$$

using the scaling technique and the reference BH mass, $9.5 \pm 1.1 M_\odot$ (for XTE J1550–564). For details, see Table 3.

3.2.2. Scaling of $\Gamma - N_{bmc}$ correlation for MAXI J1348–630

The BH mass scaling method using the $\Gamma - N_{bmc}$ correlation is described in detail in ST09. This method is aimed at: (i) searching for such a pair of BHs for which the Γ correlates with increasing N_{bmc} (which is proportional to \dot{M} , see ST09, Eqs. 4 and 7 therein) and the saturation level Γ_{sat} are the same and (ii) calculating the scaling coefficient s_N , which allows us to determine a BH mass of the target object. It is worthwhile emphasizing that we need a ratio of distances for the target and reference sources in order to estimate a BH mass using the following equation for the scaling coefficient:

$$s_N = \frac{N_r}{N_t} = \frac{m_r d_t^2}{m_t d_r^2} f_G, \quad (7)$$

where N_r, N_t are normalizations of the spectra, $m_t = M_t/M_\odot$, $m_r = M_r/M_\odot$ are the dimensionless BH masses with respect to solar, d_t and d_r are distances to the target and reference sources, correspondingly. We have a geometry factor of $f_G = \cos i_r / \cos i_t$, where i_r and i_t are the disk inclinations for the reference and target sources, respectively (see ST09, Eq. 7). We compared the difference of the disk X-ray fluxes for the reference and target sources, in the direction towards the Earth observer. We used XTE J1550–564 as the reference source.

Table 3. BH masses and distances

Reference source	$m_r^{(a)}$ (M_\odot)	$i_r^{(a)}$ (deg)	$d_r^{(b)}$ (kpc)	References
XTE J1550–564	9.5 ± 1.1	72 ± 5	2.5	Orosz et al. (2002); Sanchez-Fernandez et al. (1999)
Target source	$m_t^{(c)}$ (M_\odot)	$i_t^{(d)}$ (deg)	$d_t^{(b)}$ (kpc)	
MAXI J1348–630	14.8 ± 0.9	65 ± 5	3.4 ± 0.4	Lamer et al. (2021) and this work
	14.8 ± 0.9	75 ± 8	2.2 ± 0.6	Chauhan et al. (2021) and this work

Notes. (a) Dynamically determined BH mass and system; (b) source distance found in literature; (c) scaled value found by $\Gamma - \nu_L$ correlation, and (d) scaled value found by the $\Gamma - N_{bmc}$ correlation of the present paper.

Table 4. Parameterizations of scaling patterns for reference and target sources

Reference source	\mathcal{A}	$\Gamma - N_{bmc}$				β	Γ -QPO			
		\mathcal{B}	\mathcal{D}	N_{tr}	A		B	$\nu_{tr}(Hz)$	D	
XTE J1550-564	2.84 ± 0.08	1.8 ± 0.3	1.0	1.05 ± 0.06	0.61 ± 0.02	2.94 ± 0.08	1.27 ± 0.02	10.1 ± 0.5	1.0	
Target source	\mathcal{A}	\mathcal{B}	\mathcal{D}	N_{tr}	β	A	B	$\nu_{tr}(Hz)$	D	
MAXI J1348–630	2.96 ± 0.07	0.52 ± 0.02	1.0	1.2 ± 0.1	0.50 ± 0.03	2.93 ± 0.09	1.25 ± 0.04	6.48 ± 0.07	1.0	

Notes. We use Eqs. (3–6) for the analytical description of Γ -QPO and $\Gamma - N_{bmc}$ correlations, correspondingly.

In Fig. 8, we demonstrate the Γ versus N_{bmc} , where N_{bmc} is presented in the units of L_{39}/d_{10}^2 (L_{39} is the source luminosity in units of 10^{39} erg/s and d_{10} is the distance to the source in units of 10 kpc). As we can see, the correlations of both sources are characterized by similar shapes and saturation levels, $\Gamma_{sat} \sim 2.9 \pm 0.2$. In order to implement the scaling method, we used an analytical approximation $F(N)$ for the $\Gamma - N_{bmc}$ correlation, (see ST09):

$$F(N) = \mathcal{A} - (\mathcal{D} \cdot \mathcal{B}) \ln\{\exp[(1.0 - (N/N_{tr})^\beta)/\mathcal{D}] + 1\}, \quad (8)$$

where $N = N_{bmc}$. This function $F(N)$ is widely used for a description of the $\Gamma - N_{bmc}$ correlation [Sobolewska & Papadakis (2009), ST09, Seifina & Titarchuk (2010), Giacche et al. (2014); Seifina et al. (2014, 2016, 2017, 2018a,b)].

As a result of fitting the observed correlation by this function $F(N)$, we obtained a set of the best-fit parameters \mathcal{A} , \mathcal{B} , \mathcal{D} , N_{tr} , and β (see also Table 4). \mathcal{A} is the Γ saturation level for $\Gamma - N$ correlation and \mathcal{B} is the slope of this correlation. The parameter \mathcal{D} controls how fast the transition occurs, N_{tr} is the normalization at which the $\Gamma - N$ correlation levels off, and β is the power-law index of the part of the curve for lower argument values.

We estimated a BH mass for MAXI J1348–630 using Fig. 7. We also fit the correlation $\Gamma - N_{bmc}$ by Eq. (8) to get an estimate for $N_r^{J1348} = (1.2 \pm 0.1)$ taken at the beginning of the Γ -saturation part. We obtain $s_N = N_r/N_t$ applying N -values (see Table 4). Finally, Eq. (7) provides us a BH mass value with an accuracy of a factor f_G , namely,

$$m_t = f_G \frac{m_r d_r^2}{s_N d_t^2}. \quad (9)$$

We then obtain

$$m_t = 20 f_G \quad (10)$$

if we use values of $m_r = 9.5$, $d_t = 3.39$ kpc and $d_r = 2.5$ kpc (Table 3) and $c_N = (N_r/N_t) = 0.875$ (Table 4).

Thus, we estimate $m_t = m_{J1348}$ with an accuracy of factor f_G assuming $d_{J1348} = 3.39$ kpc (Lamer et al. 2021). We used all the parameters of the formulas in Eqs. 3 and 8 to fit the observed correlations Γ versus ν_{QPO} and Γ vs N_{BMC} (see Table 4, Figs. 7–8).

3.3. Estimate of the orbital inclination for MAXI J1348–630 using the scaling technique

Now, we estimate the inclination using a value of the geometric factor f_G . We can evaluate f_G more accurately, knowing a value of a BH mass obtained using the $\Gamma - \nu_L$ scaling [Eq. (6)] and Eq. (10) that for the $\Gamma - N$ scaling. Thus, equating a BH mass using the $\Gamma - \nu_L$ correlation (Eq. 6) to that for the $\Gamma - N$ one (Eq. 10), we found that:

$$f_G = 0.74. \quad (11)$$

Moreover, we can estimate the inclination in MAXI J1348–630 knowing the inclination i of the XTE J1550–54 (see Table 3). Indeed, since:

$$f_G = (\cos i)_{J1550} / (\cos i)_{J1348} = 0.74, \quad (12)$$

we obtain the following:

$$i_{J1348} = (65 \pm 7)^\circ. \quad (13)$$

In addition, we can evaluate a range of inclination values depending on the distance to MAXI J1348–630; for example, for a distance range of 3–5 kpc, the inclination range can be estimated using the scaling method as then would be obtained using the Lamer et al. result to be 70 – 35° . For the distance, $d_t = 2.2_{-0.6}^{+0.5}$

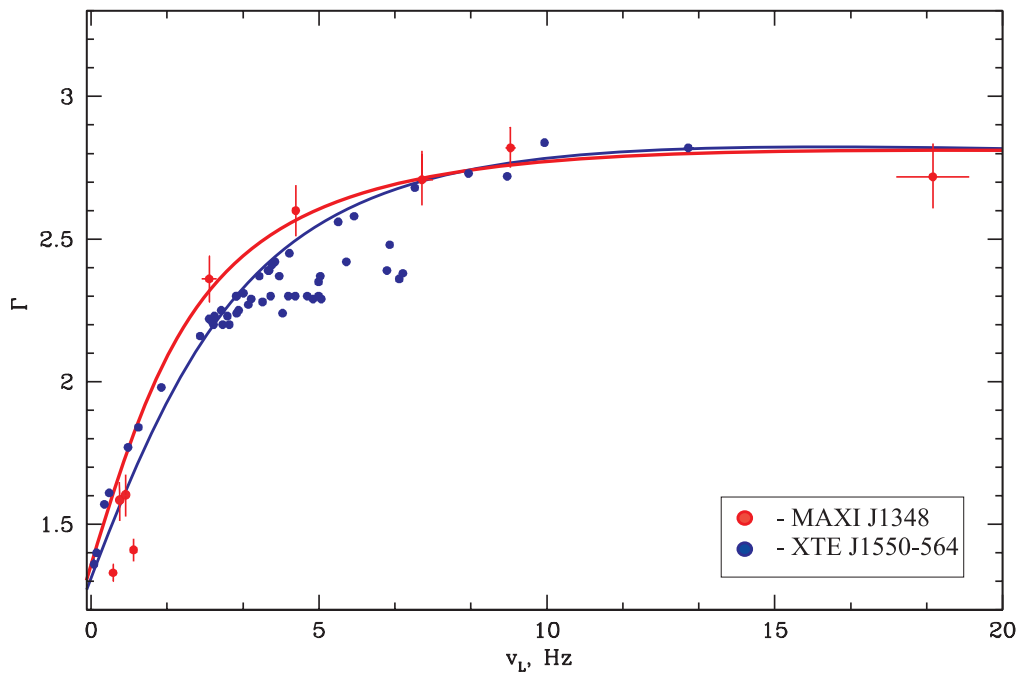


Fig. 7. Photon index, Γ , versus the QPO frequency, ν_L , for MAXI J1348–630 (target source) and XTE J1550–564 (reference source). We use a specific function $f(\nu)$, detailed in Eq. 3 of Sect. 3.2.1, to fit the data, which gives us the corresponding solid lines. We can see that Γ is correlated with ν_L and saturated for $\nu_L > 6.8$ Hz and $\nu_L > 10$ Hz for MAXI J1348–630 and XTE J1550–564, respectively. Data for XTE J1550–564 were taken from ST09.

kpc, obtained by (Chauhan et al. 2021), taking into account the large uncertainties in the source distance, we can only give a limiting range of the inclination as $75^\circ < i_t < 80^\circ$. This clearly contradicts the absence of eclipses in the observed light curve (see Fig. 3) in this binary system.

4. Discussion

The Swift/XRT data of the MAXI J1348–630 outburst are well fitted by the BMC model for all analyzed LHS, IS and HSS spectra (see Figures 4 and 6). Our results from the spectral analysis are consistent with previous results by other authors using various X-ray observations of MAXI J1348–630 [see Z20, J20 and

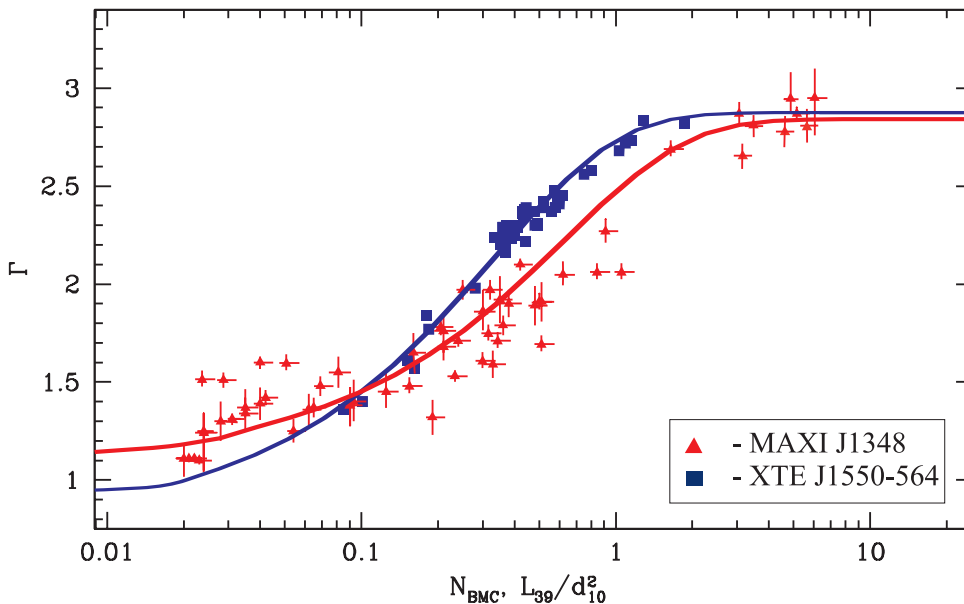


Fig. 8. Γ vs N_{bmc} correlations those for MAXI J1348–630 (target source) and for a BH XTE J1550–564 (reference source). We use a specific function, $F(N)$, (see Eq. 8) to fit the data, which gives us the corresponding solid lines.

Lamer et al. (2021)]. In particular, spectral parameter behavior observed by us is also consistent with those recently reported by Carotenuto et al. (2021b), who modeled the Swift/XRT spectra (1–10 keV) of MAXI J1348–630 using the `tbabs*powerlaw` model. They found that the index Γ changes from 1.5 to 2.4 during the outburst using their simplified model, `tbabs*powerlaw`. However, these authors could not constrain Γ during the HSS and they fixed it at 2.4 (see their Figure 2). This outcome was not by chance, as Carotenuto et al. (2021b) used the phenomenological model `tbabs*powerlaw` instead of the physical (Comptonization) model which we applied to the same data.

Tominaga et al. (2020) modeled the MAXI J1348–630 spectra detected by MAXI/GSC in 2–20 keV energy range using the `tbabs*(simple*diskbb)` model and found that Γ changes from 1.5 to 2.9 – this result is similar to ours (see our Figures 7–8). Furthermore, Tominaga et al. (2020) estimated the BH mass by applying the XSPEC `kerrbb` model and found that the values of $m_{BH} = M_{BH}/M_{\odot}$ were 7.0. It is worth pointing out that the `kerrbb` model has five main parameters for the BH mass estimate: the spinning parameter, a , inclination angle, i , and a black hole mass, m_{BH} , under a given source distance, mass accretion rate, and a spectral hardening factor. However, in our case, we used observational points of the Γ versus QPO frequency correlation and only one the best-fit parameter, m_{BH} . Our scaling method allows us to estimate m_{J1348} as 14.8 ± 0.9 , using the XTE J1550 source as a reference.

We compared our results with those obtained by Z20 based on NICER data. In Z20, the MAXI J1348–630 spectra were fitted during the outburst with the `tbnew*(diskbb + nthcomp)` model and then compared with the `tb-new*(simple*diskbb)` model results. In Z20, higher values of Γ were obtained throughout the whole outburst from MJD 58520 to 58635 ($\Gamma = 1.5 - 3.8$), as compared to our results ($\Gamma = 1.1 - 3$). In particular, at the decay phase of the outburst (MJD 58525–58597), Z20 reported that Γ decreases only from 3.5 to 3, which is very different from that found in this paper (from 3 to 1.4). Moreover, a decrease of Γ in our estimate is from 1.9 to 1.6 while in Z20 it is from 3 to 1.7 during MJD 58580–58610. Z20 found a decrease in the temperature of the inner disk

from $kT_{in} \sim 0.7$ to 0.5 keV (MJD 58520–58600), which is consistent with our results (from 0.7 to 0.4 keV). The decrease in the contribution of the Comptonized component, f , to the total flux found by Z20 from 0.6 to 0.1 (MJD 58520–58600) is also consistent with the behavior of $\log(A)$ [$f = A/(1 + A)$] (see Table A) obtained in our spectral analysis as the X-ray flux decreases. However, here we found a wider range of a decrease of f from 1 to 0.1. Again, the contribution of the Comptonized component, f , to the total flux increases up to 0.7 in Z20, which is somewhat more modest than the result we obtained: ($f \sim 1$, MJD 58600–58635). Furthermore, Z20 found a sharp decrease in kT_s from 0.5 to 0.2 keV when the source passed from the HSS to the LHS (MJD 58608), which is consistent with our results in general; however, we found a decrease in kT_s only from 0.4 to 0.3 keV. In Z20, the behavior of the spectral parameters is similar with those found in our paper. The general picture of the outburst in MAXI J1348–630 is adequately reproduced in both models (compare our Fig. 6 to Fig. 5 in Z20).

It is worth emphasizing that we have found a specific type of behavior with regard to the temperature of seed photons originating in the disk, kT_s , at the very beginning of the outburst, just before the transition to the soft state (MJD 58510–58518). The temperature, kT_s , initially decreases (from 0.45 keV to 0.2 keV) and the Comptonized fraction, f , increases from 0.75 to 0.9 during the initial rise in the low-hard state (Fig. 6). It is interesting to note that a similar behavior for kT_s was found for the same source for these MJD dates by Zhang et al. (2022), although kT_s decreased somewhat within different limits: from 0.75 to 0.5 keV. According to our spectral analysis the Comptonized fraction f , at the same time, increases from 0.75 to 0.9 during the initial rise in LHS (Fig. 6). We note that f is a parameter associated with the relative size of the corona with a respect to a distance from the soft photon source (disk). As a result, its increase in f immediately before the outburst (see panel 2 at the top of Fig. 6) simultaneously with the decrease in kT_s points to an initial increase in the corona size. Furthermore, at the end of the outburst-rise phase (HSS, MJD 58519 – 58525), the spectra further soften with an increase in the total flux along with a slight increase in the disk seed photon temperature kT_s from 0.2 to 0.75

keV. At the same time, the contribution of the Comptonized component, f , to the total flux remained almost constant, increasing from 0.9 to 1 (*blue* dots, in Fig. 6). This effect has a simple physical interpretation in terms of the BMC model (Titarchuk & Zannias 1998; Laurent & Titarchuk 1999). At the beginning of the outburst (see Fig. 6), the corona is very extended and, thus, seed photons are injected into the corona from a relatively far-away region of the disk, where the disk temperature is about 0.2–0.4 keV. As the mass accretion rate increases (or the luminosity increases), the corona contracts and consequently kT_s increases (see an illustration of this phenomenon in Fig. 2 of Seifina et al. (2014) and an analytical explanation of the evolution of the spectral index from the low hard state to softer states in black holes in Seifina et al. (2018b)). In this case, the parameter f increases sharply (from 0.7 to 0.9). It is possible that such a decrease in kT_s and a simultaneous increase in f immediately before the outburst can be considered a signature of the transition of a BH object into a flare (or of the readiness of the BH object to go into an outburst). This effect has also been observed in other black holes (e.g., GX 339–4, GRO J1655–40, 4U 1543–47, XTE J1550–564, XTE J1650–500, H 1743–322, and XTE J1859–226 [ST09], GRS 1915+105 (Titarchuk, & Seifina 2009), and 4U 1630–47 (Seifina et al. 2014) as well as in other studies of MAXI 1348 (Z22). Future observations of other BH sources that will demonstrate such behavior of kT_s and f on the eve of the flare may help verify the validity or even the universality of this signature.

Our results are also consistent, with the results of the spectral analysis by Z22 based on HXMT and *Swift* data. However, those authors find, on average, a flatter $\bar{\Gamma} \sim 2.4$, during outburst decay than our best-fit results ($\bar{\Gamma} \sim 2.7$). Perhaps the difference in Γ compared to our results is due to the different energy range, or perhaps caused by a different spectral model. Throughout the outburst, their Γ ranges from 1.3 (ID=0214002002) to 2.9 (ID=0214002065, see their Table 1). This is in full agreement with our results ($\Gamma = 1.1 - 2.9$). We note that when fitting the *Swift* data, Z22 simply fixed Γ at the canonical value during the outburst decay, $\Gamma = 2.5$, rather than looking for the best-fit solution (see their Table 2).

In Figures 7–8, we show how smoothly Γ evolves from the LHS to the HSS, with a clear indication of the saturation of Γ , that is, at least there is a sharp change in the Γ versus QPO frequency slope for high values of ν_L and high mass accretion rates, \dot{M} , respectively. This effect was predicted semi-analytically by Titarchuk & Zannias (1998) and then using Monte-Carlo simulations by Laurent & Titarchuk (1999, 2011). Moreover it was confirmed using the *RXTE* observations of Cyg X–1 (see ST07 and ST09), XTE J1859–226, XTE J1650–500, H1743–322, GX339–4, XTE J1543–47 (ST09), 4U1630–47 (Seifina et al. 2014), and GRS 1915+105 (Titarchuk, & Seifina 2009), as well as observed in our study, which allowed us to confirm the presence of a BH in MAXI J1348–630.

Using the scaling method ($\Gamma - \nu_L$) (ST07, ST09) we estimated the BH mass in MAXI J1348–630 (see Fig. 7 and Table 3). The BH mass value $14.8 \pm 0.9 M_\odot$ is relatively far from the previous BH mass estimate in MAXI J1348–630 of 7–12 M_\odot (Lamer et al. 2021; Tominaga et al. 2020), J20 and Z20, see also our Table 1 (compare Tables 1 and 3). A possible reason for the discrepancy between our estimate of a BH mass and that based on luminosity (Z20 and Lamer et al. (2021)) is an assumption by those authors that the object emits at the Eddington luminosity regime, which, in fact may not be the case. As a result, a BH mass value is naturally under-estimated.

In contrast to Z20 and Lamer et al. (2021), we determined a BH mass using the first scaling $\Gamma - \nu_L$ method and it was not necessary to know the distance to the source. Thus, the main advantages of the scaling method ($\Gamma - \nu_L$) to estimate a BH mass in comparison with other methods we used is that only one of the best-fit parameters is required, namely, a BH mass, M_{BH} , for at least nine observational points of $\Gamma - \nu_L$ (see Fig 7). It is worth noting that we also need a similar $\Gamma - \nu_L$ correlation with a known BH mass, which is that of XTE J1550–564.

We estimated the inclination, i , by combining the two scaling methods ($\Gamma - \nu_L$ and $\Gamma - N_{bmc}$). This estimate is very different from the radio inclination estimate $i_{rad} < 46^\circ$ (Carotenuto et al. 2021b). A possible reason for this discrepancy may be related to the fact that the inclination estimate from radio data is based on the difference in the brightness of the approaching jet and the receding jet based on the assumption that these jets are identical and oppositely directed, which may not necessarily be the case (Chatterjee et al. 2020; Davis & Tchekhovskoy 2020).

Another reason for this discrepancy using radio data and X-ray data is their association with different geometric scales. It is known that the radio data is mostly formed in the outer part of the source, while the X-ray emission originates in the innermost region (TL). Therefore, this estimate ($i_{rad} < 46^\circ$) may turn out to be unreliable for the inner part of the X-ray source. On the other hand, our scaling estimate [$i = (65 \pm 5)^\circ$] can be a useful alternative because we evaluate i using X-ray emission presumably originated in the TL.

5. Conclusions

We studied the spectral evolution of MAXI J1348–630 using fits of the observed X-ray emission by *Swift*/XRT. We demonstrated that the energy spectra during all spectral states could be fitted by an additive model consisting of the Comptonization (BMC) and Gaussian iron-line components. As a result, we found that Γ monotonically increased with ν_L and \dot{M} during the transition from the LHS to the HSS and then became saturated at $\Gamma \sim 2.9$ for high ν_L and \dot{M} values. We applied these correlations and found that they were similar to those established in a number of other BH candidates and could be considered as an observational evidence for the presence of a BH in MAXI J1348–630.

We estimated a BH mass for MAXI J1348–630 using the above scaling methods (see § 3.2). In particular, the $\Gamma - \nu_L$ correlation scaling method, which relies on XTE J1550–564 as a reference source, allowed us to estimate the BH mass in MAXI J1348–630 of $M_{BH} = 14.8 \pm 0.9 M_\odot$. It is important to emphasize once again that the $\Gamma - \nu_L$ correlation is independent of the distance and inclination of the object and it is therefore fairly accurate in the determination of a BH mass.

We also detected a specific decrease in the disk seed photon temperature, kT_s , at the beginning of the outburst: kT_s initially decreases from 0.4 to 0.2 keV and increases only after the source transits to the outburst rise-maximum phase. Initial decrease in kT_s occurred simultaneously with an increase in the illumination fraction, f . We interpreted this effect in terms of the Comptonization model. Since the Compton cloud (or corona) is very extended at the outburst beginning and, thus, the seed photons injected to the corona from the relatively cold and peripheral disk region, where kT_s is about 0.2–0.4 keV. While \dot{M} increases (or luminosity increases), the corona contracts and, thus, the seed photon temperature, kT_s , increases. It is possible that such a specific decrease in kT_s taking place simultaneously with an increase in the illumination fraction, f , can be considered to

be a signature of the readiness of a BH object to go into an outburst.

Acknowledgements

We acknowledge support from UK *Swift* Science Data Centre at the University of Leicester for supplied data. We thank the anonymous referee for the careful reading of the manuscript and for providing valuable comments. We are very happy to get a careful reading and editing our manuscript by Chris Shrader. This research has made using the data and/or software provided by the High Energy Astrophysics Science Archive Research Center (HEASARC), which is a service of the Astrophysics Science Division at NASA/GSFC and the High Energy Astrophysics Division of the Smithsonian Astrophysical Observatory. The data used in this paper are public and available through the GSFC public archive at <https://heasarc.gsfc.nasa.gov>. This work was made use of XRT and BAT data supplied by the UK *Swift* Science Data Centre at the University of Leicester⁴, and MAXI data was provided by RIKEN, JAXA⁵, and the MAXI team.

References

- Bassi, T., Del Santo, M., D’Ai, A., Motta, S., Marino, A., Segreto, A., 2019, *The Astronomer’s Telegram*, 12477, 1
- Borozdin, K., Revnivtsev, M., Trudolyubov, S. et al., 1999, *ApJ*, 517, 367
- Burrows D. N., Hill J. E., Nousek J. A. et al., 2005, *Space Science Reviews*, 120, 165
- Capitanio F., Belloni T., Del Santo M., Ubertini P., 2009, *MNRAS*, 398, 1194
- Carotenuto, F., Corbel, S., Tremou, E. et al., *MNRAS*, 2021a, 505, L58
- Carotenuto, F., Corbel, S., Tremou, E. et al., *MNRAS*, 2021b, 504, 444
- Chauhan, J., Miller-Jones, J., Raja, W. et al. 2021, *MNRAS*, 501, L60
- Chatterjee, K., Younsi, Z., Liska, M. et al., 2020 *MNRAS*, 499, 362
- D’ Ai, A. et al. 2007, *ApJ*, 667, 411
- Del Santo M., et al., 2016, *MNRAS*, 456, 3585
- Davis, S. & Tchekhovskoy A., 2020, *ARA&A*, 58, 407
- Ding, G.Q., Chen, T.T. & Qu, J.L. *MNRAS*, 2021, 500, 772
- Dunn R. J. H., Fender R. P., Körding E. G., Belloni T., Merloni A., 2011, *MNRAS*, 411, 337
- Giacche, S., Gili, R. & Titarchuk, L. 2014, *A&A*, 562, A44
- Filippenko, A. V., & Chornock, R. 2001, *IAU Circ.*, 7644, 2
- Greene, J., Bailyn, C. D., & Orosz, J. A. 2001, *ApJ*, 554, 1290
- Herrero, J., et al. 1995, *A&A*, 297, 556
- Hjellming, R. M., & Rupen, M. P. 1995, *Nature*, 375, 464
- Homan, J., Wijnands, R., Kong, A., Miller, J.M., Rossi, S., Belloni, T., & Lewin, W. H. G. 2006, *MNRAS*, 366, 235
- Hynes, R. I., Steeghs, D., Casares, J., Charles, P. A., & O’Brien, K. 2004, *ApJ*, 609, 317
- Evans, P. A., Beardmore, A. P., Page, K. L., et al. 2009, *MNRAS*, 397, 1177
- Evans, P.A. et al. 2007, *A&A*, 469, 379
- Fürst, F., et al., 2015, *ApJ*, 808, 122
- Homan, J., Belloni, T., 2005, *Ap&SS*, 300, 107
- Jana, A., Debnath, D., Chatterjee, D., et al. 2020, *ApJ*, 897, 3
- HI4PI Collaboration, Ben Bekhti, N., Flöer, L., et al. 2016, *A&A*, 594, A116
- Kennea, J. A. & Negoro, H., 2019, *The Astronomer’s Telegram*, 12434, 1
- Lamer, G., Schwöpe, A. D., Predehl, P., et al. 2021, *A&A*, 647, A7
- Laurent, P., & Titarchuk, L. 1999, *ApJ*, 511, 289
- Laurent, P., & Titarchuk, L. 2011, *ApJ*, 727, L34
- Long, X., Feng, H., Li, H., et al. 2022, *ApJ*, 924, L13
- Maccarone, T. J. 2003, *A&A*, 409, 697
- McClintock, J & Remillard, R 2006, *Black hole binaries*, csxs.book. pp. 157
- Miller-Jones, J. C. A., Bahramian, A., Orosz, J. A. et al. 2021, *Science*, 371, 1045
- Munoz-Darias, T., Casares, J., & Martinez-Pais, I. G. 2008, *MNRAS*, 385, 2205
- Ninkov, Z., Walker, G. A. H., & Yang, S. 1987, *ApJ*, 321, 425
- Orosz, J. A. et al. 2002, *ApJ*, 568, 84
- Nowak, M. A. 1995, *PASP*, 107, 1207
- Orosz, J. A. et al. 2002, *ApJ*, 568, 84
- Park, S. Q., et al. 2004, *ApJ*, 610, 378
- Petri, J. 2008, *Ap&SS*, 318, 181
- Russell, D. M., Baglio, C. M., & Lewis, F. 2019, *The Astronomer’s Telegram*, 12439, 1
- Sanchez-Fernandez, C., Castro-Tirado, A. J., Duerbeck, H.W., et al. 1999, *A&A*, 348, L9
- Seifina, E., Titarchuk, L. & Ugolkova, L. 2018, *A&A*, 619, 217
- Seifina, E., Chekhtman, A. & Titarchuk, L. 2018, *A&A*, 613, 48
- Seifina, E., Titarchuk, L., & Virgili, E. 2017, *A&A*, 607, A38
- Seifina, E., Titarchuk, L., & Shaposhnikov, N. 2016, *ApJ*, 821, 23
- Seifina, E. Titarchuk, L. & Shaposhnikov, N. 2014, *ApJ*, 789, 57
- Seifina, E., & Titarchuk, L. 2011, *ApJ*, 737, 128
- Seifina, E. & Titarchuk, L. 2010, *ApJ*, 722, 586
- Shaposhnikov, N., & Titarchuk, L. 2009, *ApJ*, 699, 453 (ST09)
- Shaposhnikov, N., & Titarchuk, L. 2007, *ApJ*, 663, 449
- Shaposhnikov, N. et al.. 2007, *ApJ*, 655, 434
- Shakura, N.I., & Sunyaev, R.A. 1973, *A&A*, 24, 337 (SS73)
- Shrader, C. & Titarchuk, L. G. 1999, *ApJ*, 521, L121
- Shrader, C. & Titarchuk, L. G. 2003, *ApJ*, 598, 168
- Stiele H., Kong A. K. H., 2016, *MNRAS*, 459, 4038
- Stiele, H., Belloni, T. M., Kalemci, E., & Motta, S. 2013, *MNRAS*, 429, 2655
- Sterner S. J. & Shrader C. R., 2005, *ApJ*, 625, 923
- Sobczak, G. J., McClintock, J. E., Remillard, R. A., & Bailyn, C. D. 1999, *ApJ*, 520, 776
- Sobolewska M. A. & Papadakis, I.E. 2009, *MNRAS*, 399, 1997
- Sunyaev, R.A. & Titarchuk, L.G. 1980, *A&A*, 86, 121
- Titarchuk, L.G. & Fiorito, R. 2004, *ApJ*, 612, 988
- Titarchuk, L. & Seifina, E. 2021, *MNRAS*, 501, 5659
- Titarchuk, L. & Seifina, E. 2017, *A&A*, 602, 113
- Titarchuk, L. & Seifina, E. 2016, *A&A*, 585, A94
- Titarchuk, L., Seifina, E. & Shrader, Ch. 2014, *ApJ*, 789, 98
- Titarchuk, L. & Seifina, E. 2009, *ApJ*, 701, 1463
- Titarchuk, L., Shaposhnikov, N. & Seifina, E. 2010, *AIP Conference Proceedings*, 1205, 168
- Titarchuk, L.G., Lapidus, I. & Muslimov, A. 1998, *ApJ*, 499, 315
- Titarchuk, L.G., Mastichiadis, A. & Kylafis, N.D. 1997, *ApJ*, 487, 834
- Titarchuk, L. & Zannias, T. 1998, *ApJ*, 499, 315
- Tominaga, M., Nakahira, S., Shidatsu, M., et al. 2020, *ApJ*, 899, L20
- Yatabe, F., Negoro, H., Nakajima, M., et al. 2019, *ATel*, 12425, 1
- Vahdat Motlagh, A., Kalemci, E., & Maccarone, T. J. 2019, *MNRAS*, 485, 2744
- Vaughan S., Goad M. R., Beardmore A. P., O’Brien P. T., Osborne J. P., Page K. L., Barthelmy S. D., Burrows D. N., 2006, *ApJ*, 638, 920
- Wilms, J., Allen, A., McCray, R. 2000, *ApJ*, 542, 914
- Zhang, W., Tao, L., Soria, R. et al., 2022, *ApJ*, 927, 210 (Z22)
- Zhang, L., Altamirano, D., Cúneo, V. A., Alabarta, K., Enoto, T., Homan, J., Remillard, R. A., Uttley, P. et al., 2020, *MNRAS*, 499, 851 (Z20)
- Zhang, L., Chen, L., Qu, J.-l., Bu, Q.-c., Zhang, W., 2015, *ApJ*, 813, 90

⁴ https://www.swift.ac.uk/swift_portal

⁵ <http://maxi.riken.jp/mxondem>

Appendix A: Additional table

Table A.1. Best-fit parameters[†] of the MAXI J1348–630 spectra during 2019 outburst events observed by *Swift*.

Proposal ID 00...	MJD, day	$\Gamma = \alpha + 1$	kT_s , keV	$\log(A)^{\ddagger\ddagger}$	$\nu_L^{\ddagger\ddagger\ddagger}$, Hz	$N_{\text{bmc}},$ L_{39}/d_{10}^2	$N_{\text{line}}^{\ddagger\ddagger\ddagger\ddagger}$	$E_{\text{line}},$ keV	χ_{red}^2 (dof)	Ext. ^{†††††} region
885807000	58509.47	1.11±0.01	0.40(6)	0.54(8)	...	0.02(1)	0.10(2)	6.71(5)	1.05 (710)	0–20
885960000	58510.05	1.37±0.05	0.42(3)	1.62(2)	...	0.06(1)	0.14(5)	6.62(4)	0.97 (946)	3–30
886266000	58511.58	1.53±0.03	0.32(3)	0.57(8)	...	0.23(1)	0.23(3)	6.74(7)	0.91 (958)	6–30
886496000	58512.43	1.59±0.07	0.37(4)	0.60(1)	0.56(2)	0.33(2)	0.31(2)	6.58(6)	0.89 (881)	7–30
011107001	58513.11	1.60±0.03	0.62(3)	0.64(2)	...	0.04(1)	0.29(6)	6.90(4)	1.09 (898)	10–30
088843001	58515.75	1.71±0.03	0.29(8)	0.69(1)	...	0.24(9)	0.30(4)	6.68(5)	0.98 (958)	12–30
011107002	58517.67	1.79±0.03	0.31(9)	0.74(5)	...	0.36(2)	0.27(3)	6.83(7)	1.07 (846)	12–30
011107003	58519.34	2.19±0.02	0.43(1)	0.82(2)	...	0.48(2)	0.49(4)	6.64(5)	1.06 (584)	16–30
011107004	58512.07	2.50±0.07	0.69(4)	0.95(1)	...	0.38(1)	0.52(8)	6.71(8)	1.00 (893)	31–50
011107005	58523.00	2.79±0.04	0.70(3)	1.11(2)	...	3.51(1)	0.47(6)	6.85(4)	0.96 (894)	27–50
011107006	58523.45	2.87±0.02	0.63(4)	2.00 ^{††}	...	5.64(2)	0.61(7)	6.81(5)	1.11 (552)	32–50
011107007	58524.53	2.97±0.05	0.70(2)	2.00 ^{††}	...	6.27(2)	0.84(5)	6.75(5)	1.05 (894)	33–50
011107008	58525.77	2.84±0.04	0.64(1)	2.00 ^{††}	...	5.91(3)	0.71(5)	6.73(6)	0.74 (619)	32–50
011107009	58526.25	2.85±0.05	0.69(5)	2.00 ^{††}	9.1(1)	6.05(2)	0.83(9)	6.62(9)	0.84 (525)	31–50
011107010	58527.44	2.37±0.06	0.39(2)	2.00 ^{††}	2.6(2)	4.90(2)	0.75(4)	6.40(5)	1.05 (894)	31–50
011107011	58530.29	2.68±0.03	0.71(4)	1.42(7)	4.49(1)	0.21(2)	4.52(8)	6.40(5)	1.02 (894)	31–50
011107012	58531.36	2.87±0.06	0.69(4)	1.14(5)	...	3.05(4)	3.21(6)	6.42(7)	1.06 (486)	31–50
011107013	58533.54	2.41±0.03	0.67(5)	1.09(6)	...	0.81(2)	3.05(4)	6.56(3)	0.91 (451)	30–50
011107014	58535.80	2.69±0.04	0.68(1)	1.04(1)	...	0.85(3)	0.81(5)	6.64(8)	1.09 (440)	30–50
011107015	58544.91	2.68±0.02	0.69(4)	1.02(3)	...	0.79(2)	0.74(3)	6.63(4)	1.12 (437)	26–50
011107016	58547.83	2.69±0.04	0.65(2)	1.01(2)	7.3(2)	0.62(1)	0.76(4)	6.69(9)	1.08 (455)	25–50
088843002	58550.49	2.31±0.03	0.59(6)	0.98(7)	...	0.42(3)	0.80(6)	6.68(5)	1.02 (476)	22–50
011107017	58553.87	2.49±0.05	0.57(4)	0.79(6)	...	0.32(2)	0.75(5)	6.71(7)	0.95 (426)	17–30
011107019	58559.13	2.41±0.02	0.57(1)	0.68(5)	...	0.35(2)	0.71(4)	6.62(6)	1.07 (408)	15–30
011107020	58562.05	2.41±0.02	0.55(3)	0.36(2)	...	0.51(3)	0.72(3)	6.70(4)	1.11 (424)	15–30
011107021	58565.82	2.57±0.05	0.57(4)	0.29(4)	...	0.25(2)	0.69(6)	6.67(5)	1.09 (403)	12–30
011107022	58571.40	2.70±0.07	0.55(6)	0.27(6)	18.5(8)	0.30(2)	0.63(3)	6.65(7)	1.05 (404)	12–30
011107024	58574.38	2.18±0.04	0.54(3)	0.18(2)	...	0.21(3)	0.67(4)	6.68(4)	0.96 (424)	11–30
011107025	58577.24	1.76±0.03	0.56(3)	0.15(3)	...	0.11(1)	0.61(3)	6.61(5)	1.09 (403)	12–30
011107026	58583.03	1.75±0.02	0.57(4)	0.11(6)	...	0.15(3)	0.58(6)	6.59(7)	0.95 (386)	11–30
011107027	58585.21	1.76±0.05	0.55(1)	0.08(4)	...	0.21(2)	0.54(5)	6.63(4)	0.81 (364)	11–30
011107028	58588.73	1.75±0.07	0.53(2)	0.09(3)	...	0.10(3)	0.35(4)	6.49(5)	1.08 (347)	12–30
011107029	58597.04	1.6±0.1	0.46(5)	0.08(2)	...	0.16(2)	0.18(3)	6.48(7)	1.07 (316)	10–30
011107032	58606.39	1.55±0.08	0.41(3)	0.89(5)	...	0.08(3)	0.13(6)	6.42(8)	1.10 (394)	3–30
011107033	58609.47	1.48±0.05	0.29(1)	1.10(6)	...	0.07(2)	0.11(5)	6.58(5)	1.09 (437)	0–20
011107034	58612.44	1.45±0.09	0.25(5)	1.47(9)	...	0.13(4)	0.10(4)	6.57(7)	0.97 (258)	0–20
011107035	58615.97	1.42±0.04	0.24(1)	1.54(6)	...	0.04(2)	0.14(3)	6.60(8)	1.06 (109)	0–20
011107036	58618.74	1.40±0.08	0.21(6)	2.00 ^{††}	...	0.09(3)	0.12(6)	6.69(9)	1.05 (72)	0–20
011107037	58621.39	1.51±0.04	0.26(3)	2.00 ^{††}	...	0.038(1)	0.11(3)	6.57(7)	0.86 (50)	0–20
011107038	58624.07	1.39±0.09	0.24(2)	2.00 ^{††}	...	0.04(1)	0.18(2)	6.55(7)	0.79 (45)	0–20
011107039	58627.44	1.38±0.08	0.22(1)	2.00 ^{††}	...	0.09(3)	0.13(5)	6.58(6)	0.81 (38)	0–20
011107040	58630.69	1.37±0.05	0.21(4)	2.00 ^{††}	...	0.03(1)	0.15(3)	6.61(9)	1.02 (33)	0–20
011107041	58633.15	1.36±0.08	0.23(3)	1.95(4)	...	0.06(2)	0.19(2)	6.59(8)	1.09 (221)	0–20
011107042	58639.65	1.3±0.1	0.22(1)	2.00 ^{††}	...	0.04(1)	0.11(3)	6.60(7)	1.02 (710)	0–20
011107043	58655.13	1.32±0.09	0.24(4)	2.00 ^{††}	0.9(2)	0.19(4)	0.10(4)	6.62(9)	0.94 (470)	0–20
011107044	58655.62	1.31±0.03	0.25(6)	2.00 ^{††}	0.48(1)	0.03(1)	0.18(1)	6.70(8)	0.89 (417)	0–20
011107045	58685.02	1.3±0.1	0.24(3)	2.00 ^{††}	...	0.09(2)	0.10(3)	6.71(7)	1.06 (549)	0–20
011107047	58690.13	1.25±0.06	0.25(5)	2.00 ^{††}	...	0.05(2)	0.13(2)	6.68(6)	1.05 (327)	0–20
011107048	58699.83	1.2±0.1	0.24(1)	2.00 ^{††}	...	0.02(1)	0.19(1)	6.63(7)	0.96 (59)	0–20
011107049	58706.41	1.24±0.09	0.23(5)	2.00 ^{††}	...	0.02(1)	0.12(3)	6.65(7)	0.75 (43)	0–20
011107050	58713.04	1.11±0.03	0.24(3)	2.00 ^{††}	...	0.02(1)	0.10(2)	6.60(6)	0.78 (32)	0–20
011107052	58726.99	1.10±0.05	0.23(2)	2.00 ^{††}	...	0.02(1)	0.15(3)	6.64(9)	0.74 (30)	0–20
011107055	58734.03	1.11±0.08	0.25(4)	2.00 ^{††}	...	0.02(1)	0.11(1)	6.62(4)	0.79 (30)	0–20

Notes.

[†] The spectral model is `tbabs*(bmc+gauss)`; ^{††} when the parameter $\log(A) > 1$ then this parameter is fixed at a value of 2, because for a sufficiently high $\log(A)$ (and, therefore, a high value A), the illumination factor $f = A/(1+A)$ becomes a constant value close to 1; ^{†††} the centroid frequency taken from Z20; ^{††††} normalization parameter of the Gaussian model is in units of total photons $\text{cm}^{-2} \text{s}^{-1}$ in the line and σ_{line} of *Gaussian* component is fixed to a value 0.5 keV (see comments in the text); ^{†††††} the inner and outer radii of the annulus region for the spectrum extraction is indicated in pixels (1 pixel = 2.35 arcsec).